Smoothed dissipative particle dynamics - a mesoscopic particle-based hydrodynamic technique for complex fluids

Dmitry A. Fedosov*, Kathrin Müller, and Gerhard Gompper

Theoretical Soft Matter and Biophysics, Institute of Complex Systems and Institute for Advanced Simulation, Forschungszentrum Jülich, 52425 Jülich, Germany
*E-mail: d.fedosov@fz-juelich.de

Smoothed dissipative particle dynamics (SDPD) combines two popular mesoscopic techniques, the smoothed particle hydrodynamics and dissipative particle dynamics (DPD) methods, and can be considered as an improved DPD approach. Advantages of the SDPD method over conventional DPD include the possibility of using an arbitrary equation of state, direct input of transport properties, and a well-defined physical scale of discretized elements or fluid particles. The SDPD method has been already applied to a number of mesoscopic problems involving complex fluids. Despite several advantages of the SDPD method over the conventional DPD model, the original formulation of SDPD by Español and Revenga (2003) lacks angular momentum conservation, leading to unphysical results for problems where the conservation of angular momentum is essential. To overcome this limitation, the SDPD method is extended by introducing a particle spin variable such that local and global angular momentum conservation is restored. The new SDPD formulation (SDPD+a) is directly derived from the Navier-Stokes equation for fluids with spin, while thermal fluctuations are incorporated similar to the DPD method. In this chapter, we describe the basics of the SDPD method and show several of its applications including particle margination in blood flow. In addition, the SDPD method with angular momentum conservation is validated using two problems: (i) the Taylor-Couette flow with two immiscible fluids and (ii) a tank-treading vesicle in shear flow with a viscosity contrast between inner and outer fluids. For both problems, the new SDPD method leads to simulation predictions in agreement with the corresponding analytical theories, while the original SDPD method fails to capture properly physical characteristics of the systems due to violation of angular momentum conservation.

1 Introduction

Mesoscopic hydrodynamic simulations, such as the lattice Boltzmann (LB) method[1], dissipative particle dynamics (DPD)[2–4], multi-particle collision dynamics (MPC)[5,6], smoothed particle hydrodynamics (SPH)[7,8] etc., are frequently used to investigate a wide range of problems including colloidal and polymer solutions, dynamics of microswimmers, tissue growth, and flow behavior of vesicles and cells. All these examples include mesoscopic length scales (e.g., the size of suspended particles) rendering the modeling on atomistic level impossible. A continuum approximation is also not appropriate for such problems due to the loss of necessary mesoscopic details. Thus, large scientific efforts have been invested to derive reliable and efficient mesoscopic simulation techniques, which are able to tackle a wide range of problems.

A recently established mesoscopic method, smoothed dissipative particle dynamics (SDPD)[9], combines advantages of two popular techniques namely SPH and DPD. The SDPD method for fluid flow is directly derived from the Navier-Stokes equation using a Lagrangian discretization similar to SPH, while the inclusion of thermal fluctuations in SDPD is similar to that in the DPD formalism. SDPD can also be considered as an improved DPD method. Advantages of the SDPD method over conventional DPD include

the possibility of using an arbitrary equation of state, direct input of transport properties, and a well-defined physical scale of discretized elements or fluid particles. In addition, it has been shown that the SDPD method produces proper scaling of thermal fluctuations for different fluid particle sizes[10]. The SDPD method has been already applied to a number of problems including simulations of different particles[11] and polymers[12] in a suspension, single red blood cells in tube flow[13], margination of leukocytes[14], and margination of different particles[15] in blood flow.

Despite the advantages of SDPD over the DPD method, the original SDPD formulation[9] does not conserve angular momentum, both locally and globally. Recent numerical simulations using the MPC method[16] have shown that angular momentum conservation is essential in some problems including Taylor-Couette flow with two immiscible fluids and vesicle tank-treading in shear flow. A violation of angular momentum conservation may lead to an asymmetric stress tensor and spurious unphysical torques, resulting in erroneous simulation results. To derive a consistent version of SDPD with angular momentum conservation, we introduce a spin variable, such that each SDPD particle possesses an angular velocity[17]. This idea is similar to that of the fluid particle (FPM) model[18], where every particle possesses an angular velocity; however, FPM lacks a direct connection to the discretization of the Navier-Stokes equation. Also, a spin variable has been introduced in the single-particle DPD formulation[19], where a colloidal particle can be represented by a single DPD particle with spin. Consistent SDPD formulation with angular momentum conservation is obtained by a direct discretization of the Navier-Stokes equation for a fluid with spin[20].

We will show several applications of the SDPD method. The SDPD method will be applied to the problem of micro- and nano-particle margination (i.e., particle migration toward the walls) in blood flow, which is a crucial step in drug delivery since it is a precondition for particle adhesion at the vessel walls. The importance of angular momentum conservation will be illustrated using two examples. First, the Taylor-Couette flow with two immiscible fluids is simulated showing that the extended SDPD method results in predictions in agreement with the analytical solution derived from the Navier-Stokes equation. The second problem to test the SDPD method with angular momentum conservation is a tank-treading vesicle in shear flow, which has been described theoretically by Keller and Skalak[21]. Vesicle tank-treading in shear flow corresponds to rotational motion of a membrane around the vesicle center-of-mass, while the vesicle preserves its stationary shape with a finite inclination angle. The new SDPD formulation results in predictions of vesicle inclination angles for several viscosity contrasts between inner and outer fluids in agreement with the Keller-Skalak theory[21], while the SDPD method without angular momentum conservation clearly fails to capture quantitatively correct dynamics.

2 Smoothed particle hydrodynamics

The basic equations to describe viscous fluid flow are the Navier-Stokes (NS) equations[20]. In a Lagrangian description, the NS equations take the form

$$\rho \frac{d\mathbf{v}}{dt} = -\nabla p + \eta \nabla^2 \mathbf{v} + \left(\frac{\eta}{3} + \xi\right) \nabla \nabla \cdot \mathbf{v}, \tag{1}$$

where $\mathbf{v}$ is the fluid's velocity, ρ is the fluid's density, p is the pressure, η is the dynamic shear viscosity, and ξ is the bulk viscosity. For the closure of the equations above, we also

need to add the continuity equation given by

$$\frac{d\rho}{dt} + \rho\nabla \cdot \mathbf{v} = 0. \tag{2}$$

The smoothed particle hydrodynamics (SPH) method[7,22] for fluid flow is a Lagrangian discretization of Eqs. (1) and (2). In the SPH method, a field variable $\tilde{g}(\mathbf{r})$ is replaced by the convolution integral of a field $g(\mathbf{r})$ and a kernel function $W(\mathbf{r}, h)$ as,

$$\tilde{g}(\mathbf{r}) \approx \int_V g(\mathbf{r}')W(\mathbf{r} - \mathbf{r}', h)\, dV', \tag{3}$$

where the kernel function has to be differentiable and depends on the distance $|\mathbf{r} - \mathbf{r}'|$ and the smoothing length h. In addition, the integral over $W(\mathbf{r} - \mathbf{r}', h)$ has to be normalized and the condition $\lim_{h\to 0} W(\mathbf{r} - \mathbf{r}', h) = \delta(\mathbf{r} - \mathbf{r}')$ needs to be satisfied. For $W(\mathbf{r}, h)$ being the delta function, we would have $\tilde{g}(\mathbf{r}) = g(\mathbf{r})$. The convolution integral is discretized using small fluid volumes (or particles) such that $\rho(\mathbf{r}')dV' \to m_j$ with m_j being the mass and $\rho(\mathbf{r}') \to \rho(\mathbf{r}_j)$ being the mass density of particle j at the position vector $\mathbf{r}_j$. The discretized convolution integral is then given by

$$\tilde{g}(\mathbf{r}_i) \approx \sum_{j=1}^{N} \frac{m_j}{\rho(\mathbf{r}_j)} g(\mathbf{r}_j)W(|\mathbf{r}_i - \mathbf{r}_j|, h), \tag{4}$$

where N is the number of particles (Lagrangian discretization points) within the volume V characterized by the smoothing radius h. Furthermore, derivatives of the field variable $g(\mathbf{r})$ follow similar approximation strategy which is described in Appendix A. Further in the text, we will also use the notations $\rho(\mathbf{r}_j) = \rho_j$, $g(\mathbf{r}_j) = g_j$, and $W(|\mathbf{r}_i - \mathbf{r}_j|, h) = W_{ij}$.

Using the SPH formalism, the continuity equation (2) becomes (see Eq. (31))

$$\frac{d\rho_i}{dt} = \sum_j m_j \mathbf{v}_{ij} \cdot \nabla_i W_{ij}, \tag{5}$$

where $\nabla_i W_{ij}$ can be analytically calculated. The particle density ρ_i is defined as

$$\rho_i = \sum_j m_j W_{ij}. \tag{6}$$

Hence, the density of particle i can be computed using its neighboring particles located within a sphere with a radius h. Similarly, different terms of the NS equation (1) can be discretized to obtain the equations which govern particle dynamics. Using the Newton's second law of motion $m_i d\mathbf{v}_i/dt = \mathbf{F}_i$ and the rules in Eqs. (32)-(36) of Appendix A we obtain the two forces: conservative (C) and dissipative (D) given by

$$\begin{aligned}
\mathbf{F}^C_{ij} &= \left(\frac{p_i}{\rho_i^2} + \frac{p_j}{\rho_j^2}\right) F_{ij}\mathbf{r}_{ij}, \\
\mathbf{F}^D_{ij} &= -\left(\frac{5\eta}{3} - \xi\right)\frac{F_{ij}}{\rho_i\rho_j}\mathbf{v}_{ij} - 5\left(\frac{\eta}{3} + \xi\right)\frac{F_{ij}}{\rho_i\rho_j}\hat{\mathbf{e}}_{ij}(\hat{\mathbf{e}}_{ij} \cdot \mathbf{v}_{ij}),
\end{aligned} \tag{7}$$

where p_i is the particle pressure, $\hat{\mathbf{e}}_{ij} = \mathbf{r}_{ij}/|\mathbf{r}_{ij}|$. A function $F(\mathbf{r}_{ij}) = F_{ij} \geq 0$ is defined such that $\nabla_i W_{ij} = -\mathbf{r}_{ij}F_{ij}$, and $\mathbf{F}_i = \sum_j \left(\mathbf{F}^C_{ij} + \mathbf{F}^D_{ij}\right)$, where the sum runs over all neighboring particles j of the particle i within the radius h. The conservative force controls

locally the pressure field in the system. The dissipative force provides translational friction leading to the reduction of the velocity difference between two particles.

Time evolution of the position and the velocity of a particle i follows the Newton's second law as

$$\dot{\mathbf{r}}_i = \mathbf{v}_i, \quad \dot{\mathbf{v}}_i = \mathbf{F}_i = \sum_j \frac{1}{m_j} \mathbf{F}_{ij}. \tag{8}$$

Equation (8) is integrated using the velocity-Verlet algorithm[23]. Finally, in simulations the Lucy function[7]

$$W(r) = \frac{105}{16\pi h^3} \left(1 + 3\frac{r}{h}\right) \left(1 - \frac{r}{h}\right)^3, \tag{9}$$

is often used as a kernel function, which leads to $F(r) = \frac{315}{4\pi h^5} \left(1 - \frac{r}{h}\right)^2$. The equation of state for the pressure is often chosen to be

$$p = p_0 \left(\frac{\rho}{\rho_0}\right)^\alpha + b, \tag{10}$$

where ρ_0 is the reference density, and the parameters p_0, α, and b can be freely selected. This pressure equation yields the speed of sound $c^2 = p_0\alpha/\rho_0$, which can be easily controlled through the above parameters resulting in a good approximation of fluid incompressibility[22,24].

3 Smoothed dissipative particle dynamics

The smoothed dissipative particle dynamics (SDPD) method proposed by Español and Revenga[9] is a mesoscopic particle-based hydrodynamic approach which has been derived from the SPH[7,22] and DPD[2,3] simulation methods. Thus, in addition to the hydrodynamics described by SPH, consistent thermal fluctuations (i.e., they satisfy a balance between dissipative and random contributions) similar to those in the DPD method have to be added. To derive the random contribution, it is convenient to represent the dissipative force in Eq. (7) in a tensorial form as $\mathbf{F}^D_{ij} = -\boldsymbol{\mathcal{T}}_{ij} \cdot \mathbf{v}_{ij}$, where $\boldsymbol{\mathcal{T}}_{ij} = A(r_{ij})\mathbb{1} + B(r_{ij})\hat{\mathbf{e}}_{ij}\hat{\mathbf{e}}_{ij}$ and

$$A(r_{ij}) = \left(\frac{5\eta}{3} - \xi\right) \frac{F_{ij}}{\rho_i \rho_j} \quad \text{and} \quad B(r_{ij}) = 5\left(\frac{\eta}{3} + \xi\right) \frac{F_{ij}}{\rho_i \rho_j}. \tag{11}$$

Following the general framework of the fluid particle model[18], a random force can be defined as

$$\tilde{\mathbf{F}}_{ij} dt = \sqrt{2k_B T} \left(\tilde{A}(r_{ij}) d\overline{\boldsymbol{\mathcal{W}}}^S_{ij} + \frac{\tilde{B}(r_{ij})}{3} \mathrm{tr}[d\boldsymbol{\mathcal{W}}_{ij}]\mathbb{1} + \tilde{C}(r_{ij}) d\boldsymbol{\mathcal{W}}^A_{ij} \right) \cdot \hat{\mathbf{e}}_{ij}, \tag{12}$$

where $d\boldsymbol{\mathcal{W}}_{ij}$ is a matrix of independent Wiener increments, $\mathrm{tr}[d\boldsymbol{\mathcal{W}}_{ij}]$ is the trace of this matrix, $d\overline{\boldsymbol{\mathcal{W}}}^S_{ij} = \frac{1}{2}(d\boldsymbol{\mathcal{W}}_{ij} + d\boldsymbol{\mathcal{W}}_{ji}) - \frac{1}{3}\mathrm{tr}[d\boldsymbol{\mathcal{W}}_{ij}]$ is the traceless symmetric part, and $d\boldsymbol{\mathcal{W}}^A_{ij} = \frac{1}{2}(d\boldsymbol{\mathcal{W}}_{ij} - d\boldsymbol{\mathcal{W}}_{ji})$ is the antisymmetric part. The functions $\tilde{A}(r)$, $\tilde{B}(r)$, and $\tilde{C}(r)$ are related to $A(r)$ and $B(r)$ of the tensor $\boldsymbol{\mathcal{T}}_{ij}$ as $A(r) = (\tilde{A}(r)^2 + \tilde{C}(r)^2)/2$ and

$B(r) = (\tilde{A}(r)^2 - \tilde{C}(r)^2)/2 + (\tilde{B}(r)^2 - \tilde{A}(r)^2)/3$. To further simplify the expression in Eq. (12), we can select $\tilde{C}(r) = 0$ leading to

$$\tilde{A}(r_{ij}) = \left(2\left(\frac{5\eta}{3} - \xi\right)\frac{F_{ij}}{\rho_i\rho_j}\right)^{1/2} \quad \text{and} \quad \tilde{B}(r_{ij}) = \left(2\left(\frac{5\eta}{3} + 8\xi\right)\frac{F_{ij}}{\rho_i\rho_j}\right)^{1/2}. \quad (13)$$

The combination of forces in Eqs. (7) and (12) constitute the SDPD method, which describes hydrodynamics with consistent thermal fluctuations. The evolution of particle position and velocity follows Eq. (8). The derivation of SDPD in Ref.[9] also includes an energy conservation equation, which we omit here for simplicity. Note that this formulation violates the conservation of angular momentum, which can be essential in some physical problems (several examples will follow). The SDPD method without angular momentum conservation[9] will be called **SDPD-a**.

4 SDPD with angular momentum conservation

In SDPD, dissipative and random forces possess not only a part along the inter-particle axis as in DPD, but also a component perpendicular to the inter-particle axis. This perpendicular part of dissipative and random forces destroys local and global angular momentum conservation. There exist a version of the SDPD method with angular momentum conservation[25], where the perpendicular component of dissipative and random forces has been neglected resulting in a method formulation very similar to DPD. In this method the input viscosity has to be scaled by a theoretically defined coefficient which depends on space dimension. However, it is advantageous to keep a perpendicular component of the dissipative force, since it provides much more efficient control over fluid transport properties than the component along inter-particle axis alone[26].

To extend the original SDPD formulation[9], we introduce a spin variable for every particle ω_i. In addition, each particle will also possess a moment of inertia I_i analogously to the already defined particle mass. In order to obtain discretized equations for the SDPD formulation with spin, we consider the NS equation with spin[27],

$$\rho\frac{d\mathbf{v}}{dt} = -\nabla p + (\eta + \eta_r)\nabla^2\mathbf{v} + \left(\frac{\eta}{3} + \xi - \eta_r\right)\nabla\nabla\cdot\mathbf{v} + 2\eta_r\nabla\times\omega, \quad (14)$$

where η_r is the rotational viscosity and ω is the spin angular velocity. The introduced spin variable can be interpreted in two different ways. On the one hand, it is an approach used to recover angular momentum conservation in the SDPD formulation. On the other hand, the spin can be thought of as an effective angular velocity of a fluid volume represented by a particle. However, it should not be confused with a molecular spin. The discretization of the NS equation with spin provides a consistent model, where translational and rotational friction interactions are properly balanced unlike the FPM model which does not have a direct connection to the NS equation.

Following the rules for derivatives in Appendix A we obtain the three forces: conser-

vative (C), dissipative (D), and rotational (R) given by

$$\begin{aligned}
\mathbf{F}_{ij}^C &= \left(\frac{p_i}{\rho_i^2}+\frac{p_j}{\rho_j^2}\right) F_{ij}\mathbf{r}_{ij},\\
\mathbf{F}_{ij}^D &= -\left(\frac{5\eta}{3}+3\eta_r-\xi\right)\frac{F_{ij}}{\rho_i\rho_j}\mathbf{v}_{ij} \;-5\left(\frac{\eta}{3}+\xi-\eta_r\right)\frac{F_{ij}}{\rho_i\rho_j}\hat{\mathbf{e}}_{ij}(\hat{\mathbf{e}}_{ij}\cdot\mathbf{v}_{ij}),\\
\mathbf{F}_{ij}^R &= -2\eta_r\frac{F_{ij}}{\rho_i\rho_j}\mathbf{r}_{ij}\times(\boldsymbol{\omega}_i+\boldsymbol{\omega}_j)\,.
\end{aligned} \tag{15}$$

The conservative and dissipative forces are very similar to the expressions in Eq. (7). In addition, now we have a rotational force which is also dissipative, but acts on particles' angular velocities such that a spin of one particle leads to a change in translational and angular velocity of another particle.

The defined set of deterministic forces in Eq. (15) can be referred to as a SPH discretization with angular momentum conservation. However, the SDPD method also incorporates consistently thermal fluctuations by appending a random force to the set of forces in Eq. (15). Here, the combination of dissipative, rotational, and random forces has to satisfy the fluctuation-dissipation balance. Similarly to the dissipative force, we re-write the rotational force in a tensorial form as $\mathbf{F}_{ij}^R = -\boldsymbol{\mathcal{T}}_{ij}\cdot(\mathbf{r}_{ij}\times(\boldsymbol{\omega}_i+\boldsymbol{\omega}_j))/2$. Note that the same tensor $\boldsymbol{\mathcal{T}}_{ij}$ is used for both dissipative and rotational forces in order to satisfy the fluctuation-dissipation theorem when a random force is added[18]. This implies that $\eta_r = 5\eta/3-\xi$ and

$$A(r_{ij}) = 4\left(\frac{5\eta}{3}-\xi\right)\frac{F_{ij}}{\rho_i\rho_j}, \quad \text{and} \quad B(r_{ij}) = 10\left(\xi-\frac{2\eta}{3}\right)\frac{F_{ij}}{\rho_i\rho_j}. \tag{16}$$

Then, the corresponding functions for the random force in Eq. (12) are given by

$$\tilde{A}(r_{ij}) = \left(2\left(\frac{20\eta}{3}-4\xi\right)\frac{F_{ij}}{r_i r_j}\right)^{1/2} \quad \text{and} \quad \tilde{B}(r_{ij}) = \left(2\left(17\xi-\frac{40\eta}{3}\right)\frac{F_{ij}}{r_i r_j}\right)^{1/2}. \tag{17}$$

The full set of forces for the SDPD method with angular momentum conservation is finally given by

$$\begin{aligned}
\mathbf{F}_{ij}^C &= \left(\frac{p_i}{\rho_i^2}+\frac{p_j}{\rho_j^2}\right) F_{ij}\mathbf{r}_{ij},\\
\mathbf{F}_{ij}^D &= -\left(\gamma_{ij}^a\left(\mathbf{v}_{ij}+\frac{\hat{\mathbf{e}}_{ij}\left(\hat{\mathbf{e}}_{ij}\cdot\mathbf{v}_{ij}\right)}{3}\right)\right)-\frac{2\gamma_{ij}^b}{3}\hat{\mathbf{e}}_{ij}\left(\hat{\mathbf{e}}_{ij}\cdot\mathbf{v}_{ij}\right),\\
\mathbf{F}_{ij}^R &= -\gamma_{ij}^a\frac{\mathbf{r}_{ij}}{2}\times\left(\boldsymbol{\omega}_i+\boldsymbol{\omega}_j\right),\\
\tilde{\mathbf{F}}_{ij} &= \left(\sigma_{ij}^a d\overline{\boldsymbol{\mathcal{W}}}_{ij}+\sigma_{ij}^b\frac{1}{3}tr[d\boldsymbol{\mathcal{W}}_{ij}]\mathbb{1}\right)\cdot\frac{\hat{\mathbf{e}}_{ij}}{dt},
\end{aligned} \tag{18}$$

where

$$\gamma_{ij}^a = \left(\frac{20\eta}{3}-4\xi\right)\frac{F_{ij}}{\rho_i\rho_j}, \quad \gamma_{ij}^b = \left(17\xi-\frac{40\eta}{3}\right)\frac{F_{ij}}{\rho_i\rho_j}, \tag{19}$$

and $\sigma_{ij}^{a,b} = 2\sqrt{k_B T \gamma_{ij}^{a,b}}$. It is important to note that these equations are only valid for $2\eta/3 \leq \xi \leq 5\eta/3$, such that the friction coefficients $(\gamma_{ij}^a + 2\gamma_{ij}^b)/3$ and γ_{ij}^a are positive. Another simplification which can be made is the reduction to a single dissipative parameter γ_{ij} such that $\xi = 20\eta/21$ and

$$\gamma_{ij}^a = \gamma_{ij}^b = \gamma_{ij} = \frac{20\eta}{7}\frac{F_{ij}}{\rho_i \rho_j}, \qquad \sigma_{ij}^a = \sigma_{ij}^b = \sigma_{ij} = 2\sqrt{k_B T \gamma_{ij}}. \tag{20}$$

The derived SDPD method with angular momentum conservation will be referred to as **SDPD+a** further in text. To describe time evolution of the position and of the translational and angular velocity of a particle i, Eq. (8) with an addition of angular velocity integration ($\dot{\boldsymbol{\omega}}_i = \sum_j \mathbf{N}_{ij}/I_j$) is employed, where $\mathbf{N}_{ij}$ is the torque exerted by particle j on particle i and is given by $\mathbf{N}_{ij} = \mathbf{r}_{ij} \times \mathbf{F}_{ij}/2$. This leads to local and global angular momentum conservation. More details on the SDPD method with angular momentum conservation can be found in Ref.[17].

5 Application of the SDPD method

The SDPD method has been used in simulations of colloidal particles[11] and polymers[12], single red blood cells in tube flow[13], margination of leukocytes[14], and margination of micro- and nano-particles[15] in blood flow.

5.1 Margination of micro- and nano-particles in blood flow

The first step in the delivery of small drug carriers is their transport along blood vessels which determines their initial distribution. Further, the distribution of micro- and nano-particles is affected by their binding to specific targeted sites. However, efficient binding of carriers can be achieved only if they are present near vessel walls at sufficiently high concentrations, and thus, the distribution of micro- and nano-carriers within vessel cross-sections plays an essential role in their efficient delivery. The cross-sectional distribution of micro- and nano-particles depends on local blood flow properties such as hematocrit (volume fraction of red blood cells) and flow rate as well as on the particle characteristics such as their size, shape, and deformability. The migration of various suspended particles toward walls in blood flow, which is also often referred to as *margination*, has been observed for white blood cells[28,29,14], platelets[30,31], and rigid micro-particles[32,33]. Particle margination in blood flow is mediated by red blood cells (RBCs), which migrate to the vessel center[34] due to hydrodynamic interactions with the walls (called lift force)[35–37], and lead to an increased concentration of different particles within the RBC-free layer (RBCFL) near a wall (a layer void of RBCs). More precisely, the margination mechanism is a consequence of the competition between lift forces on RBCs and suspended particles, and their interactions in flow[38]. Similarly, micro- and nano-carriers have a potential to get marginated[15], and therefore to interact with vessel walls.

Numerical simulations of blood flow on a single-cell level allow us to explore the flow behavior and interaction of blood cells and other suspended components[39–41]. Thus, the role of particle size and shape on the margination efficiency can be investigated *in silico*[15] providing information about particle adhesion potential, since particle margination

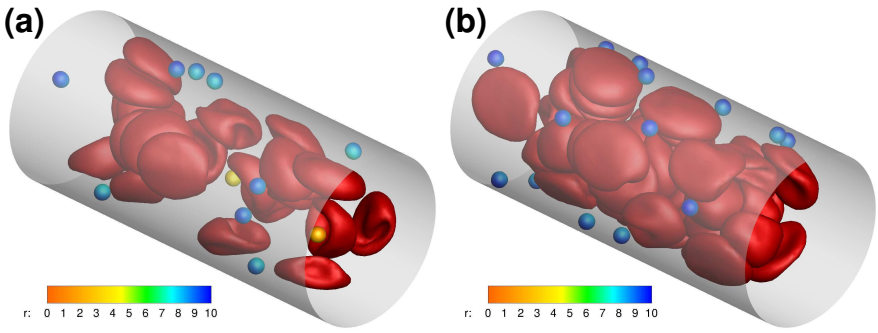

Figure 1. Particle distributions in blood flow. Illustrations of 3D simulations of blood flow for different hematocrit values (a) $H_t = 0.2$ and (b) $H_t = 0.4$. RBCs are drawn in red, while spherical carriers with a size of $D_p = 1.83\,\mu$m are colored according to their radial position r. For better contrast, carrier positions from several time instances are superimposed in the plots.

is an essential pre-condition for particle adhesion. The findings in Ref.[15] indicate that spherical particles have slightly better margination properties than ellipsoids, however the adhesion efficiency of ellipsoidal particles appears to be superior in comparison with that of spheres due to a larger area for adhesive interactions[42]. The larger particles possess a larger probability of being marginated. As the particle size becomes very small (less than about $100 - 200$ nm), the particle distribution within vessel cross-section can be described well by the volume of blood plasma, since small particles are uniformly distributed within the suspending fluid.

The simulations are based on the SDPD-a method. Blood is modeled as a suspension of RBCs and micro- or nano-particles. RBCs and suspended micro- and nano-particles are modeled by a collection of particles on their surface connected by viscoelastic springs. The membrane model also incorporates bending resistance and the area and volume conservation constraints. For full details about the membrane model and simulation conditions and setup we refer the reader to Ref.[15].

Margination of micro- and nano-particles in blood flow depends on hematocrit H_t, vessel diameter, and flow rate[15]. Figure 1 illustrates the distribution of carriers with a diameter $D_p = 1.83\,\mu$m for two H_t values. For better visibility, the carrier positions from a few snapshots are superimposed in the plot. The carrier surfaces are colored according to their radial position in the channel, with yellow color indicating a position near the channel center, while blue color corresponds to a position near the wall. Clearly, the carriers are marginating better for the case of larger H_t.

Carrier positions in blood flow sampled over time lead to particle distributions, which reflect the probability of a particle to be at a certain distance from the wall. Figure 2 shows several center-of-mass distributions of circular particles in 2D with $D_p = 1.83\,\mu$m for several H_t values. The RBC-free layer (RBCFL) thickness, which is computed from simulation snapshots through the analysis of the RBC core boundary[43] similar to experimental measurements[44], is depicted by small arrows. The distributions have been averaged over the halves of the channel due to symmetry. Figure 2 shows that the carriers migrate into the RBCFL and remain quasi-trapped there. With increasing H_t, the carriers marginate

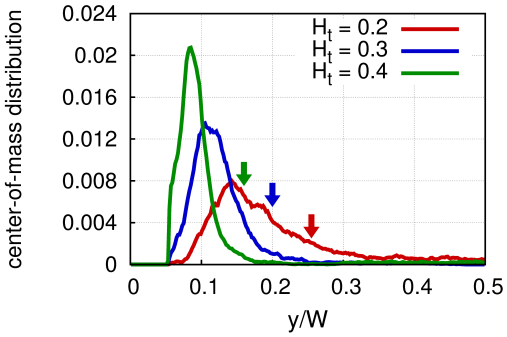

Figure 2. Center-of-mass distributions of carriers for various H_t values. 2D simulation results for circular particles with $D_p = 1.83\,\mu\text{m}$. The wall is at $y/W = 0$, where W is the channel width. The arrows indicate the boundary of the RBCFL for the different hematocrits, marked by corresponding colors.

better, as indicated by the development of a strong peak in the distribution near the wall at $y/W = 0$ (W is the channel width), and the motion of the peak position towards the wall. This is due to a decrease in the RBCFL thickness leading to a smaller available space for the particles. This trend is in agreement with experimental observations[32] and simulations[45–47] of margination of blood platelets, which have a comparable size. Further details on micro- and nano-particle margination in blood flow depending on various conditions can be found in Ref.[15].

5.2 Taylor-Couette flow of two immiscible fluids

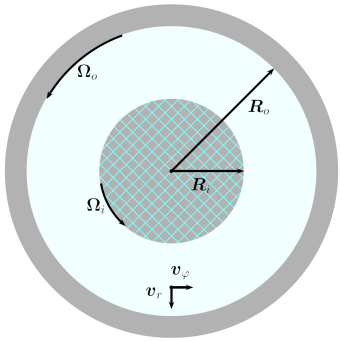

Figure 3. A sketch of two cylinders with radii R_o and R_i where the subscripts 'o' and 'i' denote the outer and inner cylinders, respectively. The gap between cylinders is filled with a fluid colored in blue. Taylor-Couette flow can be generated by rotation of the outer cylinder with a rotational frequency Ω_o. In simulations with two immiscible fluids, the inner cylinder (shaded area) is replaced by another fluid which cannot mix with the fluid inside the gap between two cylindrical surfaces.

To illustrate the importance of angular momentum conservation, we test the SDPD

method on Taylor-Couette flow, which usually refers to a fluid flow in the gap between two rotating cylinders as shown in Fig. 3. However, we consider a setup, where the inner cylinder is replaced by another immiscible fluid such that no mixing between the two fluids at R_i can occur. A solution of the incompressible NS equation for this problem yields a linear angular velocity profile $v_\phi(r) = \Omega_0 r$ across both immiscible fluids, where r is the radial position. Note that this solution is independent of the viscosity values of the immiscible fluids.

Recent numerical simulations with a similar setup[16] have shown that the conservation of angular momentum is necessary to obtain correct velocity and torque profiles across immiscible fluids with different viscosities. In simulations, the ratio of fluid viscosities was set to $\eta_i/\eta_o = 3$. The computational domain was assumed to be periodic in the cylinder-axis direction, while the cylinder wall was modeled by a layer of frozen particles with a thickness h whose structure (e.g., radial distribution function) was the same as that of the fluids. To prevent mixing of the fluids and particle penetration into the wall, specular reflection of particles has been imposed at cylindrical surfaces with $r = R_i$ and $r = R_o$. The wall particles were rotated with a constant angular frequency Ω_o in order to generate flow. Figure 4 shows angular velocity profiles for the Taylor-Couette flow using both SDPD+a and SDPD-a methods. The SDPD+a simulation properly captures a linear profile of angular velocity, while the SDPD-a method leads to distinct slopes within the regions of different viscosities.

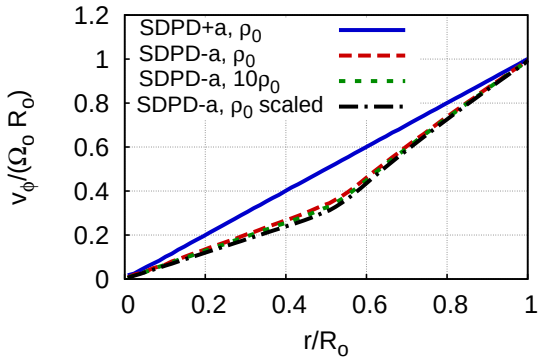

Figure 4. Angular velocity v_ϕ profiles for the Taylor-Couette flow with two immiscible fluids using both SDPD+a and SDPD-a methods. Radial position r is normalized by the cylinder radius R_o, while angular velocity is scaled with the cylinder angular velocity $\Omega_o R_o$. The SDPD+a method leads to a correct linear profile, while the SDPD-a method fails to do so due to violation of angular momentum conservation. The SDPD-a results for different resolution with $\rho = 10\rho_0$ and for a twice larger system size (marked as "scaled") show hardly any dependence on fluid resolution.

6 Tank-treading of a vesicle in shear flow

Flow dynamics of soft deformable objects such as liquid droplets, lipid vesicles, red blood cells, and elastic capsules has attracted a lot of scientific interest recently due to a wide

range of possible applications. For instance, a number of experiments[36,48], theoretical approaches[21,49,50], and simulations[50–52,39] have shown that fluid vesicles exhibit a rich dynamical behavior in shear flow including tank-treading (TT) and tumbling (TB) motion. The tumbling motion corresponds to vesicle rotation around its center-of-mass nearly as a rigid body. A tank-treading vesicle in shear flow shows a stationary shape with a finite inclination angle $\theta > 0$ with respect to the flow direction, while the membrane is rotating around the center-of-mass of the vesicle, see Fig. 5. The occurrence of different vesicle motion is governed by the viscosity contrast $\lambda = \eta_i/\eta_o$ between fluids inside and outside the vesicle with viscosities η_i and η_o, respectively. A physical explanation for the TT-to-TB transition can be derived from the two components of shear flow: an elongational part which tends to stretch and align a vesicle along the $x = y$ axis with an inclination angle of $\theta = \pi/4$ and a rotational part of the flow which exerts a torque on the vesicle membrane. Increasing of viscosity contrast leads to higher shear stresses inside the vesicle opposing its TT motion, which results in an effective torque and decrease of the vesicle inclination angle. Thus, for high enough λ a transition from TT to TB motion occurs. Keller and Skalak (KS)[21] derived a theory which predicts the TT-to-TB transition. Moreover, the KS theory is able to predict the inclination angle θ in the vesicle TT regime. Details of the KS theory are given in Appendix B.

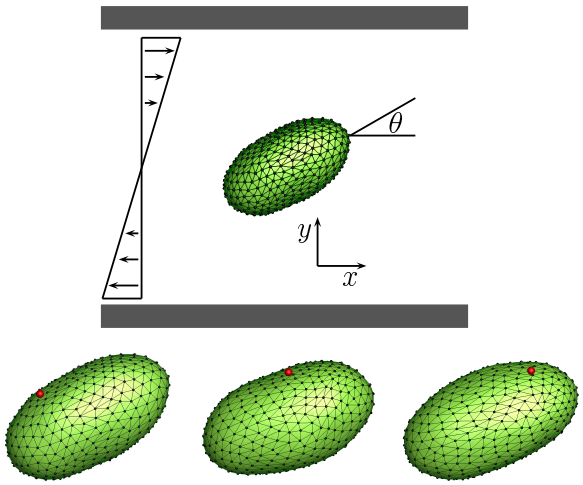

Figure 5. Simulation snapshots of a tank-treading vesicle in shear flow for $\lambda = 2$. A xy-plane view, where the flow is in x direction. The red sphere is attached to a fixed position on a vesicle in order to illustrate the TT motion of the membrane; however, it is just a marker used for visualization and introduced at post-processing stage. Note that small shape fluctuations are clearly visible.

The vesicle membrane is modeled by a collection of particles on an ellipsoidal surface. An illustration of a vesicle structure is shown in Fig. 5. The model incorporates membrane bending rigidity, the constraints for vesicle area and volume, and the viscosity contrast between inner and outer fluids; more details on vesicle modeling can be found in Ref.[17]. The simulated ellipsoidal vesicle has a prolate shape with $a_1 > a_2 = a_3$ and an aspect ratio of $a_1/a_2 \approx 1.7$. The vesicle is placed in a box, where periodic boundary conditions

are applied in x and z direction, while shear flow is generated in the x direction, as shown in Fig. 5.

The inclination angle of a TT vesicle in shear flow is calculated by

$$\theta = \arctan(u_y/u_x), \tag{21}$$

where $\mathbf{u} = (u_x, u_y, u_z)$ is the eigenvector of the moments of inertia tensor with the smallest eigenvalue. Figure 6 compares inclination angles obtained from simulations with SDPD+a and SDPD-a fluids and from the KS theory for different viscosity ratios λ. The simulation results obtained with a SDPD+a fluid agree very well with the KS theory predictions, while the results using a SDPD-a fluid show a significant overestimation of the inclination angle at large λ. The results for $\lambda = 1$ from both SDPD+a and SDPD-a cases coincide indicating that angular momentum conservation does not affect simulation results if inner and outer fluids have the same viscosity. The deviations of the SDPD+a results from the KS theory predictions might be due to small shape fluctuations of the vesicle and/or numerical errors indicated by error bars in Fig. 6.

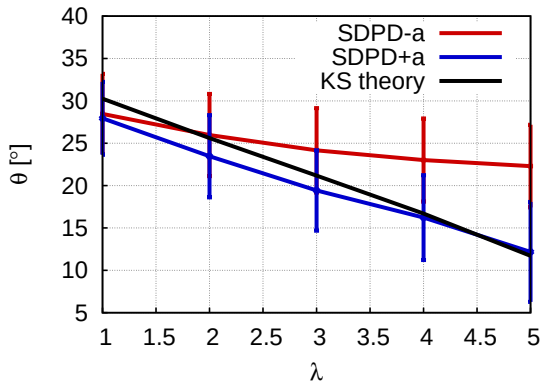

Figure 6. Comparison of inclination angles θ of a TT vesicle in shear flow obtained from SDPD+a (blue) and SDPD-a (red) simulations and from the KS theory (black) for different viscosity ratios λ.

7 Summary

We presented an overview of the SDPD-a method[9] and its extension[17], which satisfies local and global angular momentum conservation. In the SDPD+a, each particle possesses an angular velocity, and its rotational contribution has been derived from the NS equation with spin following the SPH formalism. This leads to a spin variable similar to the FPM model[18]. Thermal fluctuations in SDPD+a have been also included similar to those in FPM [18]. Several applications of the SDPD method have been considered. The first example concerned the margination of micro- and nano-particles in blood flow, which is important in drug delivery. Simulations of Taylor-Couette flow with two immiscible fluids show that SDPD+a leads to correct predictions of flow profiles in agreement with analytical results,

while SDPD-a fails to capture properly flow characteristics due to violation of angular momentum conservation. Finally, simulations of vesicle dynamics in shear flow reveal that angular momentum conservation is essential to obtain correct results for the inclination angle of a tank-treading vesicle if there exists a viscosity contrast λ between inner and outer fluids. For $\lambda \neq 1$ the SDPD+a method predicts vesicle characteristics in agreement with the KS theory for a vesicle in shear flow, while SDPD-a overestimates the inclination angle. In conclusion, the family of SDPD methods including the version with angular momentum conservation provides valuable tools for modeling flows of complex fluids.

Acknowledgments

This work has been supported by the DFG Research Unit FOR 1543 SHENC – Shear Flow Regulation in Hemostasis. Dmitry A. Fedosov acknowledges funding by the Alexander von Humboldt Foundation. Kathrin Müller acknowledges support by the International Helmholtz Research School of Biophysics and Soft Matter (IHRS BioSoft). We also gratefully acknowledge a CPU time grant by the Jülich Supercomputing Center.

Appendix

A Calculation of derivatives

We summarize the calculation of derivatives of field variables similar to those in SPH[22]. Using Eq. (4), the first derivative of a field g can be approximated as

$$\frac{\partial \tilde{g}}{\partial x} = \sum_{j=1}^{N} \frac{m_j}{\rho_j} g \frac{\partial W_{ij}}{\partial x_i}, \tag{22}$$

where the notations are identical to those in the main text. A disadvantage of this approximation is that the derivative does not vanish for g being a constant function. Therefore, a better approximation is given by

$$\frac{\partial \tilde{g}}{\partial x} = \frac{1}{\phi} \left(\frac{\partial (\tilde{g}\phi)}{\partial x} - \tilde{g} \frac{\partial \phi}{\partial x} \right), \tag{23}$$

where ϕ must be a differentiable function. Following Eq. (22), we then obtain

$$\frac{\partial \tilde{g}}{\partial x} = \frac{1}{\phi_i} \sum_{j=1}^{N} \frac{m_j}{\rho_j} \phi_j \left(g_j - g_i \right) \frac{\partial W_{ij}}{\partial x_i}. \tag{24}$$

When $\phi = 1$, Eq. (24) reduces to

$$\frac{\partial \tilde{g}}{\partial x} \approx \sum_{j} \frac{m_j}{\rho_j} g_{ji} \frac{\partial W_{ij}}{\partial x_i}, \tag{25}$$

where $g_{ji} = g_j - g_i$. In Eq. (24), $\phi = \rho$ can be also selected, yielding an approximation for the first derivative as

$$\frac{\partial \tilde{g}}{\partial x} \approx \frac{1}{\rho_i} \sum_{j} m_j g_{ji} \frac{\partial W_{ij}}{\partial x_i}. \tag{26}$$

The choice for different discretizations ($\phi = 1$ or $\phi = \rho$) may depend on a problem of interest. For instance, when different interacting fluids with large density ratios are considered, it has been shown that the approximation in Eq. (24) with $\phi = 1$ is more accurate than that with $\phi = \rho$, because ρ in Eq. (25) is included directly inside the sum[53,22]. Furthermore, if only a single fluid is employed, an approximation $\phi_i \approx \rho_j$ can be used making the above choices for ϕ equivalent.

There exists another definition for the first derivative,

$$\frac{\partial \tilde{g}}{\partial x} = \phi \left(\frac{\partial}{\partial x} \left(\frac{\tilde{g}}{\phi} \right) + \frac{\tilde{g}}{\phi^2} \frac{\partial \phi}{\partial x} \right). \tag{27}$$

Following the SPH formalism[22] we obtain

$$\frac{\partial \tilde{g}}{\partial x} \approx \phi_i \sum_{j=1}^{N} \frac{m_j}{\rho_j} \left(\frac{g_j}{\phi_j} + \frac{g_i}{\phi_i^2} \phi_j \right) \frac{\partial W_{ij}}{\partial x_i}. \tag{28}$$

As a result, a choice of $\phi = 1$ here leads to

$$\frac{\partial \tilde{g}}{\partial x} \approx \sum_{j=1}^{N} \frac{m_j}{\rho_j} \left(g_j + g_i \right) \frac{\partial W_{ij}}{\partial x_i}, \tag{29}$$

while for $\phi \approx \rho$ Eq. (28) becomes

$$\frac{\partial \tilde{g}}{\partial x} \approx \rho_i \sum_{j=1}^{N} m_j \left(\frac{g_j}{\rho_j^2} + \frac{g_i}{\rho_i^2} \right) \frac{\partial W_{ij}}{\partial x_i}. \tag{30}$$

A set of equations above defines different approximations of first derivatives, which can be used to derive discretizations of other differential operators in the NS equation. For instance, using Eq. (26) the gradient of $g(\mathbf{r})$ can be approximated as

$$\nabla \tilde{g} \approx -\frac{1}{\rho_i} \sum_j m_j g_{ij} \nabla_i W_{ij}, \tag{31}$$

where $g_{ij} = g_i - g_j$. Similarly, the divergence and the curl of a vector field $\tilde{\mathbf{G}}(\mathbf{r})$ are discretized as

$$\nabla_i \cdot \tilde{\mathbf{G}}_i \approx -\frac{1}{\rho_i} \sum_j m_j \mathbf{G}_{ij} \cdot \nabla_i W_{ij}, \tag{32}$$

$$\nabla_i \times \tilde{\mathbf{G}}_i \approx -\rho_i \sum_j \frac{m_j}{\rho_i \rho_j} \left(\mathbf{G}_j + \mathbf{G}_i \right) \times \nabla_i W_{ij}. \tag{33}$$

The second derivatives are then given by

$$\nabla_i \left(\nabla_i \cdot \tilde{\mathbf{G}}_i \right) \approx -\sum_j m_j \frac{F_{ij}}{\rho_i \rho_j} \left(5 \hat{\mathbf{e}}_{ij} \left(\hat{\mathbf{e}}_{ij} \cdot \mathbf{G}_{ij} \right) - \mathbf{G}_{ij} \right) \tag{34}$$

and

$$\nabla_i^2 \tilde{g}_i \approx -2 \sum_j m_j \frac{F_{ij}}{\rho_i \rho_j} g_{ij}, \tag{35}$$

where $\hat{\mathbf{e}}_{ij} = \mathbf{r}_{ij} / r_{ij}$ is the unity vector along the separation direction of particles i and j[9].

The curl of a vector field $\mathbf{G}$ can be approximated as

$$\nabla_i \times \tilde{\mathbf{G}}_i \approx \phi_i \sum_j \frac{m_j}{\rho_j} \nabla_i W(r_{ij}) \times \left(\frac{\mathbf{G}_j}{\phi_j} + \frac{\phi_j \mathbf{G}_i}{\phi_i^2} \right), \tag{36}$$

where a selection of $\phi = 1$ leads to

$$\nabla_i \times \tilde{\mathbf{G}}_i \approx \sum_j \frac{m_j}{\rho_j} \nabla_i W(r_{ij}) \times (\mathbf{G}_j + \mathbf{G}_i), \tag{37}$$

while $\phi = \rho$ results in

$$\nabla_i \times \tilde{\mathbf{G}}_i \approx \rho_i \sum_j m_j \nabla_i W(r_{ij}) \times \left(\frac{\mathbf{G}_j}{\rho_j^2} + \frac{\mathbf{G}_i}{\rho_i^2} \right). \tag{38}$$

B Keller-Skalak theory

The Keller-Skalak (KS) theory[21] assumes a fixed ellipsoidal shape $(r_1/a_1)^2 + (r_2/a_2)^2 + (r_3/a_3)^2 = 1$, where $r_i, i \in \{1, 2, 3\}$ are the Cartesian coordinates and a_i are the semiaxes of the ellipsoid. The motion of a vesicle is derived by considering energy balance between the energy supplied by the fluid and the energy which dissipates on the membrane and inside the vesicle. This balance leads to a differential equation given by

$$\frac{d\theta}{dt} = \frac{1}{2}\dot{\gamma}\left(B\cos(2\theta) - 1\right), \tag{39}$$

where $\dot{\gamma}$ is the shear rate. If $B > 1$, the vesicle is in the TT regime, and hence, a steady inclination angle can be found as $\theta = 0.5 \arccos(1/B)$, where B is a function of vesicle shape and viscosity contrast given by

$$\begin{aligned}
B &= f_0 \left(f_1 + \frac{1}{f_1} \left(\frac{1}{1 + f_2(\lambda - 1)} \right) \right), \\
f_0 &= \frac{2}{a_1/a_2 + a2_/a_1}, \\
f_1 &= 0.5\left(a_1/a_2 - a_2/a_1\right), \\
f_2 &= 0.5 g(\alpha_1^2 + \alpha_2^2), \\
g &= \int_0^\infty (\alpha_1^2 + s)^{-3/2} (\alpha_2^2 + s)^{-3/2} (\alpha_3^2 + s)^{-1/2}\, ds, \\
\alpha_i &= \frac{a_i}{a_1 a_2 a_3}.
\end{aligned} \tag{40}$$

Note that the KS theory does not consider vesicle's membrane viscosity.

References

1. S. Succi, *The Lattice Boltzmann equation for fluid dynamics and beyond*, Oxford University Press, Oxford, 2001.

2. P. J. Hoogerbrugge and J. M. V. A. Koelman, *Simulating microscopic hydrodynamic phenomena with dissipative particle dynamics*, Europhys. Lett., **19**, 155–160, 1992.
3. P. Español and P. Warren, *Statistical mechanics of dissipative particle dynamics*, Europhys. Lett., **30**, 191–196, 1995.
4. R. D. Groot and P. B. Warren, *Dissipative particle dynamics: bridging the gap between atomistic and mesoscopic simulation*, J. Chem. Phys., **107**, 4423–4435, 1997.
5. A. Malevanets and R. Kapral, *Mesoscopic model for solvent dynamics*, J. Chem. Phys., **110**, 8605–8613, 1999.
6. G. Gompper, T. Ihle, D. M. Kroll, and R. G. Winkler, *Multi-particle collision dynamics: a particle-based mesoscale simulation approach to the hydrodynamics of complex fluids*, Adv. Polym. Sci., **221**, 1–87, 2009.
7. L. B. Lucy, *A numerical approach to the testing the fission hypothesis*, Astronom. J., **82**, 1013–1024, 1977.
8. J. J. Monaghan, *Smoothed particle hydrodynamics*, Annu. Rev. Astron. Astrophys., **30**, 543–574, 1992.
9. P. Español and M. Revenga, *Smoothed dissipative particle dynamics*, Phys. Rev. E, **67**, 026705, 2003.
10. A. Vázquez-Quesada, M. Ellero, and P. Español, *Consistent scaling of thermal fluctuations in smoothed dissipative particle dynamics*, J. Chem. Phys., **130**, 034901, 2009.
11. X. Bian, S. Litvinov, R. Qian, M. Ellero, and N. A. Adams, *Multiscale modeling of particle in suspension with smoothed dissipative particle dynamics*, Phys. Fluids, **24**, 012002, 2012.
12. S. Litvinov, M. Ellero, X. Hu, and N. A. Adams, *Smoothed dissipative particle dynamics model for polymer molecules in suspension*, Phys. Rev. E, **77**, 066703, 2008.
13. D. A. Fedosov, M. Peltomäki, and G. Gompper, *Deformation and dynamics of red blood cells in flow through cylindrical microchannels*, Soft Matter, **10**, 4258–4267, 2014.
14. D. A. Fedosov and G. Gompper, *White blood cell margination in microcirculation*, Soft Matter, **10**, 2961–2970, 2014.
15. K. Müller, D. A. Fedosov, and G. Gompper, *Margination of micro- and nano-particles in blood flow and its effect on drug delivery*, Sci. Rep., **4**, 4871, 2014.
16. I. O. Götze, H. Noguchi, and G. Gompper, *Relevance of angular momentum conservation in mesoscale hydrodynamics simulations*, Phys. Rev. E, **76**, 046705, 2007.
17. K. Müller, D. A. Fedosov, and G. Gompper, *Smoothed dissipative particle dynamics with angular momentum conservation*, J. Comp. Phys., **281**, 301–315, 2015.
18. P. Español, *Fluid particle model*, Phys. Rev. E, **57**, 2930–2948, 1998.
19. W. Pan, I. V. Pivkin, and G. E. Karniadakis, *Single-particle hydrodynamics in DPD: a new formulation*, Europhys. Lett., **84**, 10012, 2008.
20. S. R. de Groot and P. Mazur, *Non-equilibrium thermodynamics*, North-Holland, Amsterdam, 1962.
21. S. R. Keller and R. Skalak, *Motion of a tank-treading ellipsoidal particle in a shear flow*, J. Fluid Mech., **120**, 27–47, 1982.
22. J. J. Monaghan, *Smoothed particle hydrodynamics*, Rep. Prog. Phys., **68**, 1703–1759, 2005.
23. M. P. Allen and D. J. Tildesley, *Computer simulation of liquids*, Clarendon Press, New

York, 1991.
24. G. K. Batchelor, *An introduction to fluid dynamics*, Cambridge University Press, Cambridge, 2000.
25. X. Y. Hu and N. A. Adams, *Angular-momentum conservative smoothed particle dynamics for incompressible viscous flows*, Phys. Fluids, **18**, 101702, 2006.
26. C. Junghans, M. Praprotnik, and K. Kremer, *Transport properties controlled by a thermostat: an extended dissipative particle dynamics thermostat*, Soft Matter, **4**, 156–161, 2008.
27. D. W. Condiff and J. S. Dahler, *Fluid mechanical aspects of antisymmetric stress*, Phys. Fluids, **7**, 842–854, 1964.
28. U. Bagge and R. Karlsson, *Maintenance of white blood cell margination at the passage through small venular junctions*, Microvasc. Res., **20**, 92–95, 1980.
29. H. L. Goldsmith and S. Spain, *Margination of leukocytes in blood flow through small tubes*, Microvasc. Res., **27**, 204–222, 1984.
30. G. J. Tangelder, H. C. Teirlinck, D. W. Slaaf, and R. S. Reneman, *Distribution of blood platelets flowing in arterioles*, Am. J. Physiol., **248**, H318–H323, 1985.
31. B. Woldhuis, G. J. Tangelder, D. W. Slaaf, and R. S. Reneman, *Concentration profile of blood platelets differs in arterioles and venules*, Am. J. Physiol., **262**, H1217–H1223, 1992.
32. A. W. Tilles and E. C. Eckstein, *The near-wall excess of platelet-sized particles in blood flow: its dependence on hematocrit and wall shear rate*, Microvasc. Res., **33**, 211–223, 1987.
33. E. C. Eckstein, A. W. Tilles, and F. J. Millero III, *Conditions for the occurrence of large near-wall excesses of small particles during blood flow*, Microvasc. Res., **36**, 31–39, 1988.
34. H. L. Goldsmith, G. R. Cokelet, and P. Gaehtgens, *Robin Fahraeus: evolution of his concepts in cardiovascular physiology*, Am. J. Physiol., **257**, H1005–H1015, 1989.
35. I. Cantat and C. Misbah, *Lift force and dynamical unbinding of adhering vesicles under shear flow*, Phys. Rev. Lett., **83**, 880–883, 1999.
36. M. Abkarian, C. Lartigue, and A. Viallat, *Tank treading and unbinding of deformable vesicles in shear flow: determination of the lift force*, Phys. Rev. Lett., **88**, 068103, 2002.
37. S. Messlinger, B. Schmidt, H. Noguchi, and G. Gompper, *Dynamical regimes and hydrodynamic lift of viscous vesicles under shear*, Phys. Rev. E, **80**, 011901, 2009.
38. A. Kumar and M. D. Graham, *Mechanism of margination in confined flows of blood and other multicomponent suspensions*, Phys. Rev. Lett., **109**, 108102, 2012.
39. D. A. Fedosov, H. Noguchi, and G. Gompper, *Multiscale modeling of blood flow: from single cells to blood rheology*, Biomech. Model. Mechanobiol., **13**, 239–258, 2014.
40. J. B. Freund, *Numerical simulation of flowing blood cells*, Annu. Rev. Fluid Mech., **46**, 67–95, 2014.
41. D. A. Fedosov, M. Dao, G. E. Karniadakis, and S. Suresh, *Computational biorheology of human blood flow in health and disease*, Ann. Biomed. Eng., **42**, 368–387, 2014.
42. P. Decuzzi and M. Ferrari, *The adhesive strength of non-spherical particles mediated by specific interactions*, Biomaterials, **27**, 5307–5314, 2006.
43. D. A. Fedosov, B. Caswell, A. S. Popel, and G. E. Karniadakis, *Blood flow and cell-*

free layer in microvessels, Microcirculation, **17**, 615–628, 2010.
44. S. Kim, R. L. Kong, A. S. Popel, M. Intaglietta, and P. C. Johnson, *Temporal and spatial variations of cell-free layer width in arterioles*, Am. J. Physiol., **293**, H1526–H1535, 2007.
45. L. Crowl and A. L. Fogelson, *Analysis of mechanisms for platelet near-wall excess under arterial blood flow conditions*, J. Fluid Mech., **676**, 348–375, 2011.
46. H. Zhao and E. S. G. Shaqfeh, *Shear-induced platelet margination in a microchannel*, Phys. Rev. E, **83**, 061924, 2011.
47. D. A. Reasor Jr, M. Mehrabadi, D. N. Ku, and C. K. Aidun, *Determination of critical parameters in platelet margination*, Ann. Biomed. Eng., **41**, 238–249, 2013.
48. V. Kantsler and V. Steinberg, *Transition to tumbling and two regimes of tumbling motion of a vesicle in shear flow*, Phys. Rev. Lett., **96**, 036001, 2006.
49. R. Tran-Son-Tay, S. P. Sutera, and P. R. Rao, *Determination of red blood cell membrane viscosity from rheoscopic observations of tank-treading motion*, Biophys. J., **46**, 65–72, 1984.
50. H. Noguchi and G. Gompper, *Dynamics of fluid vesicles in shear flow: effect of the membrane viscosity and thermal fluctuations*, Phys. Rev. E, **72**, 011901, 2005.
51. A. Yazdani and P. Bagchi, *Three-dimensional numerical simulation of vesicle dynamics using a front-tracking method*, Phys. Rev. E, **85**, 056308, 2012.
52. H. Zhao and E. S. G. Shaqfeh, *The dynamics of a vesicle in simple shear flow*, J. Fluid Mech., **674**, 578–604, 2011.
53. A. Colagrossi and M. Landrini, *Numerical simulation of interfacial flows by smoothed particle hydrodynamics*, J. Comp. Phys., **191**, 448–475, 2003.